In Situ Synthesis of Magnetic Field-Responsive Hemicellulose Hydrogels for Drug Delivery

Weifeng Zhao,[†,‡] Karin Odelius,[†] Ulrica Edlund,[†] Changsheng Zhao,[‡] and Ann-Christine Albertsson*,[†]

[†]Fiber and Polymer Technology, School of Chemical Science and Engineering, Royal Institute of Technology (KTH), Teknikringen 56-58 SE-100 44, Stockholm, Sweden

[‡]College of Polymer Science and Engineering, State Key Laboratory of Polymer Materials Engineering, Sichuan University, 610065, Chengdu, China

S *Supporting Information*

ABSTRACT: A one-pot synthetic methodology for fabricating stimuli-responsive hemicellulose-based hydrogels was developed that consists of the in situ formation of magnetic iron oxide (Fe_3O_4) nanoparticles during the covalent cross-linking of O-acetyl-galactoglucomannan (AcGGM). The Fe_3O_4 nanoparticle content controlled the thermal stability, macrostructure, swelling behavior, and magnetization of the hybrid hydrogels. In addition, the magnetic field-responsive hemicellulose hydrogels (MFRHHs) exhibited excellent adsorption and controlled release profiles with bovine serum albumin (BSA) as the model drug. Therefore, the MFRHHs have great potential to be utilized in the biomedical field for tissue engineering applications, controlled drug delivery, and magnetically assisted bioseparation. Magnetic field-responsive hemicellulose hydrogels, prepared using a straightforward one-step process, expand the applications of biomass-derived polysaccharides by combining the renewability of hemicellulose and the magnetism of Fe_3O_4 nanoparticles.

Magnetic Field-Responsive Hemicellulose Hydrogels
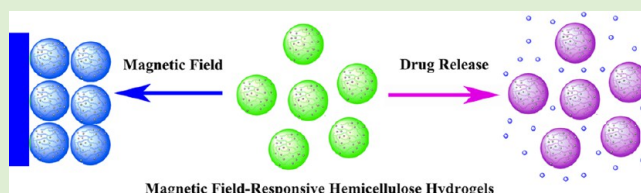
1. INTRODUCTION

Hydrogels are cross-linked hydrophilic polymeric networks that can retain a considerable amount of water or biological fluids in their porous structure while maintaining their structure.[1−3] Hydrogels from natural materials, particularly those from renewable sources, are attracting considerable attention in a variety of fields to achieve sustainable development. Polysaccharide-based hydrogels typically exhibit valuable properties, such as biodegradability, biocompatibility, eco-friendliness, low cost, easy availability and biological functions, making them promising materials for a range of applications. Among the natural polysaccharides, hemicelluloses such as O-acetyl-galactoglucomannan (AcGGM) are particularly interesting due to their good solubility in both water (green solvent) and organic solvents, in addition to the general advantages of polysaccharides mentioned above.[4−6] Hemicelluloses belong to a family of heteropolysaccharides and constitute one of the main components of plant cell walls. Hemicelluloses may be considered a renewable biopolymer resource with the potential to replace current petrochemical-based materials for positive economic and ecological impacts.

Due to their excellent optical, mechanical, and magnetic properties, magnetic nanoparticles have received considerable interest in the areas of magnetic storage media,[7] ferrofluids,[8] bimetallic nanoparticles catalysts,[9] and in biomedicine and technology (including photothermal therapy,[10] targeted drug delivery,[11−15] and contrast agents in magnetic resonance imaging[16,17]). Superparamagnetic iron oxide nanoparticles (Fe_3O_4) are the primary focus in the field of magnetic

nanoparticles due to their larger magnetic moments, excellent superparamagnetism, and high stability in aqueous media.[18] A combination of Fe_3O_4 nanoparticles and polysaccharide hydrogels can be utilized as magnetic field-responsive hydrogels. Brain-resembling, superabsorbent hydrogel composites have been produced via UV-induced copolymerization-cross-linking of vinyl-modified starch with functional monomers in the presence of Fe_3O_4 particles for use as oral drug-delivery systems.[19] Composite hydrogels of $Fe_3O_4@Au$ and κ-carrageenan were fabricated for the controlled release of methylene blue.[20] Magnetic $Fe_3O_4@SiO_2$ starch-*graft*-poly-(acrylic acid) hydrogels were prepared and used as adsorbents for the removal of crystal violet from aqueous solutions to avoid secondary pollution.[21] A new organic/inorganic hybrid was generated through the self-assembly of cholesterol-bearing pullulan hydrogels and Fe_3O_4 nanoparticles for potential application in magnetic hyperthermia therapy.[22] A promising xylan/poly(acrylic acid) magnetic hydrogel adsorbent for water treatment applications was prepared from wheat straw xylan and Fe_3O_4 nanoparticles.[23] Thermoresponsive and pH-sensitive magnetic nanohydrogels with low toxicity and enhanced anticancer effects have been developed using biodegradable starch-maleate as a cross-linker and a magnetic nanoparticle stabilizer.[24] Covalent TiO_2-*co*-pectin microspheres containing Fe_3O_4 nanoparticles were developed using an ultrasound-

Scheme 1. Proposed Synthesis of Magnetic Field-Responsive Hemicellulose Hydrogels in Basic Media
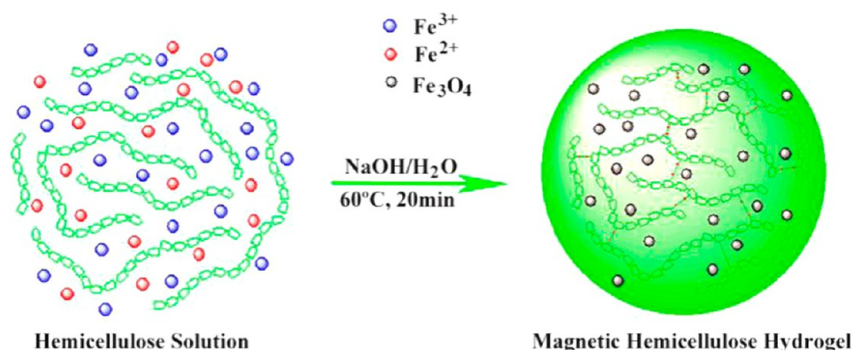
induced cross-linking/polymerization reaction, resulting in a material with the potential for use in biological environments.[25] However, multistep reactions of these organic/inorganic composite hydrogels as well as their tedious purification may limit their use. Therefore, a facile approach for the preparation of magnetic field-responsive polysaccharide hydrogels is desired.

Hemicellulose hydrogels can be prepared through either covalent or physical cross-linking. A hybrid hydrogel was prepared from hemicelluloses, poly(vinyl alcohol), and chitin nanowhiskers using the freeze—thaw technique, and this hydrogel exhibited promising properties for tissue engineering applications.[26] Hemicellulose/poly(2-hydroxyethyl methacrylate) (PHEMA)-based hydrogels were prepared via the radical polymerization of HEMA with hemicellulose specifically modified with well-defined amounts of methacrylic functions using a redox initiator system.[27] Recently, the fabrication of hemicellulose-based hydrogels has focused on endowing them with stimuli-responsive properties. A series of monomers were grafted in a controlled/living polymerization from the prepared hemicellulose macroinitiator to prevent gelation in aqueous solution.[28] To address current global environmental and resource problems, ionic renewable hydrogels based on xylan-rich hemicelluloses offer multiple responses to pH, ions, and organic solvents, and exhibit properties applicable in adsorption, separation, and drug-release systems.[29] A temperature-sensitive hemicellulose hydrogel exhibited tunable swelling behavior and morphology, implying their potential as smart materials for medical applications.[30] A pH-sensitive and biodegradable hemicellulose-based hydrogel was prepared by grafting AAc to hemicellulose as a powerful carrier for controlled drug delivery.[31] In our recent study, a robust pathway for the synthesis of electrically conductive hemicellulose hydrogels (ECHHs) based on AcGGM and a conductive aniline tetramer was reported, and these hydrogels exhibited broad potential for biomedical applications.[32] To prepare ECHHs using a more facile and greener approach, a one-pot reaction in water at ambient temperature was developed and resulted in gels with controllable conductivity, tunable swelling behavior, and acceptable mechanical properties.[33] More recently, covalent cross-linking during spray drying offered the potential for the green fabrication of microgels that exhibited a rapid stimuli response and good blood compatibility, providing a platform for stimuli-responsive hemicellulose microgels (SRHMGs).[34] To expand the applications of a biomass-derived polysaccharide by combining the renewability, biocompatibility, and biodegradability of hemicellulose and the magnetism of Fe_3O_4 nanoparticles, we were inspired to

functionalize hemicelluloses with magnetic field-responsive properties using a straightforward one-step process.

Our aim was to develop and demonstrate a one-pot pathway for fabricating stimuli-responsive hemicellulose hydrogels via the in situ formation of magnetic Fe_3O_4 nanoparticles during the covalent cross-linking of hemicellulose. We propose that the content of Fe_3O_4 nanoparticles can be employed to tune the thermal stability, macrostructure, swelling behavior and magnetization of the hybrid hydrogels. In addition, the protein adsorption and release profiles of the magnetic field-responsive polysaccharide hydrogels could be controlled.

2. EXPERIMENTAL SECTION

2.1. Materials. $FeCl_2$ and $FeCl_3 \cdot 6H_2O$ were purchased from Aladdin Chemical Company, Inc. (China) and were used as the metal ion sources. Sodium hydroxide (NaOH), epichlorohydrin (ECH) and bovine serum albumin (BSA) was obtained from Sigma-Aldrich Chemical Co. AcGGM originating from spruce (*Picea abies*) was extracted from thermo-mechanical pulping (TMP) processed water, purified and concentrated by ultrafiltration (membrane cutoff 1 kDa) and lyophilized using a Lyolab 300 lyophilizer. The carbohydrate composition of the AcGGM isolate was 17 mol % glucose, 65 mol % mannose, and 15 mol % galactose. AcGGM had a number-average molecular weight (M_n) of approximately 7500 g mol^{-1} (DP ∼ 40), a dispersity of 1.3, and a degree of acetylation of 30%, as determined by size exclusion chromatography calibrated with MALDI-TOF.[35] All of the other chemical reagents were of analytical grade, purchased from Xiya Reagent (China), and used without further purification.

2.2. Preparation of Magnetic Field-Responsive Hemicellulose Hydrogels (MFRHHs). Magnetic field-responsive hemicellulose hydrogels (MFRHHs) were prepared using a one-pot reaction with varying feed compositions, as shown in Scheme 1 and Table 1. The

Table 1. Composition of Hemicellulose Hydrogels with a Base Content of 200 mg AcGGM

sample	Fe_3O_4 content (%, w/w)	$FeCl_2$ (mg)	$FeCl_3 \cdot 6H_2O$ (mg)	NaOH (mg)	ECH (mg)	water (mL)
M-0	0	0	0	200	200	2
M-5	5	13.2	36.0	200	200	2
M-10	10	26.4	72.0	200	200	2
M-15	15	39.6	108.0	200	200	2

reaction and a detailed scheme of the cross-linking reaction involving an alkaline-mediated deprotonation of polysaccharide hydroxyls and ring opening of epichlorohydrin is shown in Schemes S1 and S2 in the Supporting Information.

Briefly, 200 mg of AcGGM was dissolved in 1 mL of a 2.5 M NaOH aqueous solution. Then, epichlorohydrin (200 mg) was added to the resulting solution as a cross-linker. The desired amounts of $FeCl_3 \cdot 6H_2O$ and $FeCl_2$ (molar ratio of $Fe^{3+}:Fe^{2+}$ = 2:1) were each dissolved in 1 mL of water. The solution containing iron ions was

added to the AcGGM solution followed by rapid evacuation to remove the bubbles formed during stirring. The cross-linking reaction was conducted at 60 °C for 20 min, and the formed gels were washed with deionized water for 48 h to remove the unreacted reagents, such as NaOH and metal ions. The deionized water was changed frequently. The MFRHHs were maintained in deionized water prior to further characterization. The Fe_3O_4 nanoparticles were prepared in the same manner without adding hemicellulose and epichlorohydrin.

The MFRHHs with 5, 10, and 15% (w/w) Fe_3O_4 nanoparticles were annotated according to their equivalents of % (w/w) of Fe_3O_4 nanoparticles as calculated from the loading of Fe ions during synthesis (Table 1). For example, M-5 contained 5% (w/w) Fe_3O_4 nanoparticles. Hydrogels without Fe_3O_4 nanoparticles were synthesized as reference samples and denoted as M-0.

2.3. Characterization. The size and morphology of the Fe_3O_4 nanoparticles were investigated using a transmission electron microscope (TEM, FEI Tecnai F20) at an accelerating voltage of 200 kV. The specimens were prepared by dropping the nanoparticles dispersed in ethanol onto carbon-coated copper microgrids followed by drying under a UV lamp.

FTIR spectroscopy was employed to confirm the molecular structure of the hemicellulose hydrogels in the dry state. The IR spectra were recorded as the average of 16 scans at a resolution of 4 cm^{-1} between 4000 and 600 cm^{-1} using an ATR-FTIR (PerkinElmer Spectrum).[36]

The thermal stability (thermogravimetric analysis, TGA) of the hydrogels in the dry state was investigated from 30 to 900 °C at a heating rate of 5 °C/min under a dry nitrogen atmosphere (flow rate of 50 mL/min) using a TG209F1 (Netzsch, Germany). Approximately 15 mg of each sample was placed into a 70 μL ceramic cup without a lid.

The swelling ratio (SR) of the hydrogels was determined by immersing the dry hydrogels in buffer solutions (prepared from Na_2HPO_4 and NaH_2PO_4, pH = 7.2−7.4) at room temperature. The masses of the samples in the swollen state $(m_{s,t})$ at different time points were measured after gently removing excess water with filter paper. The SR was calculated using eq 1:

$$SR(\%) = \frac{m_{s,t} - m_d}{m_d} \times 100 \tag{1}$$

where m_d denotes the masses of the samples in the dry state.

The cross-sectional morphology of the hydrogels was observed using a JSM-7500F (JEOL, Japan) at a voltage of 5 kV. The fully swollen samples were lyophilized overnight in small vials, cross-sectioned, attached to the sample supports using carbon tape, and coated with a 7 nm gold layer.

The magnetization value of the hemicellulose hydrogels in unit mass was investigated using a Lakeshore 7410 vibrating sample magnetometer (VSM) with an applied magnetic field of 2.0 T at room temperature to detect the room temperature magnetic hysteresis loops. For each sample, the data were collected at magnetic fields in the range of ±500 kA m^{-1} to determine the magnetization.

The hemicellulose hydrogels (∼30 mg in the dried state) were immersed in 10 mL of a BSA solution (3 mg/mL). The resulting mixture was continuously shaken at 200 rpm at room temperature for 12 h, and then the hybrid hydrogels were removed magnetically. The protein concentration in the solution was analyzed with a UV spectrophotometer (Shimadzu UV-160A, Japan) at 280 nm. The protein adsorption loading of the microspheres was calculated according to the mass balance before and after adsorption, as expressed in the following equation:

$$Q_e = \frac{c_0 - c_e}{W} \times V \tag{2}$$

where Q_e is the BSA adsorption capacity onto the unit amount of the hydrogel (mg/g), C_0 is the initial BSA concentration (mg/mL), C_e is the final or equilibrium BSA concentration (mg/mL), V is the volume of BSA solution (mL), and W is the dry weight of the hydrogel (mg).

The protein release profile on the hemicellulose hydrogels was determined in the same manner.

3. RESULTS AND DISCUSSION

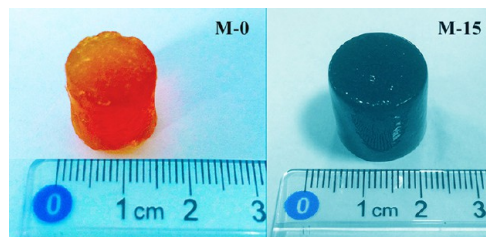Magnetic field-responsive hemicellulose hydrogels (MFRHHs) were prepared by combining the magnetism of Fe_3O_4

Figure 1. Freshly prepared hemicellulose hydrogel (M-0) and magnetic field-responsive hemicellulose hydrogel (M-15).
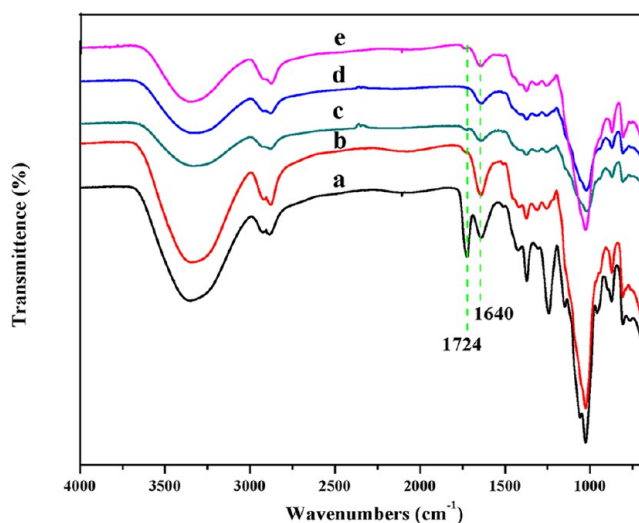

Figure 2. ATR-FTIR spectra of AcGGM (a), M-0 hydrogel (b), M-5 hydrogel (c), M-10 hydrogel (d), and M-15 hydrogel (e).
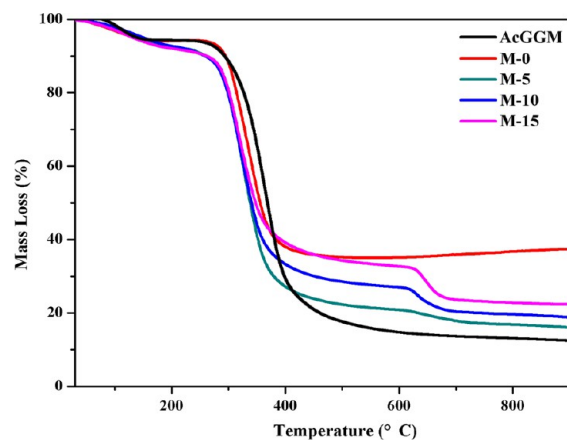

Figure 3. TGA thermograms of AcGGM, M-0, M-5, M-10, and M-15.

nanoparticles and the biocompatibility and renewability of hemicellulose AcGGM. The powerful chemical coprecipitation method produced Fe_3O_4 nanoparticles with an average size of 5.8 nm, which was confirmed by SEM and TEM observations, as shown in Figures S1 and S2 (Supporting Information). The
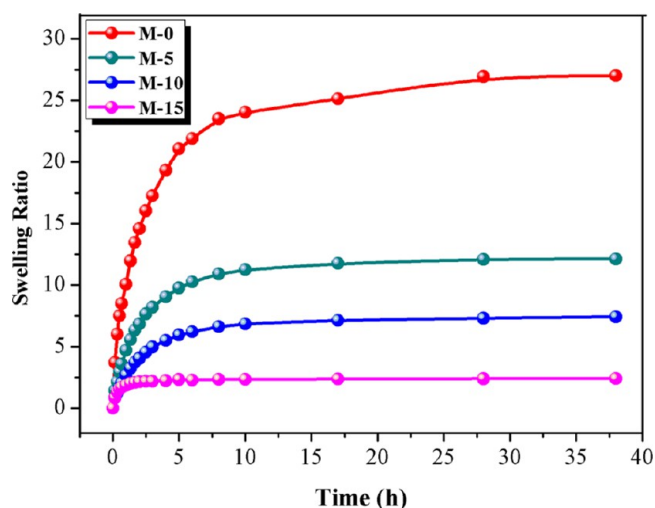
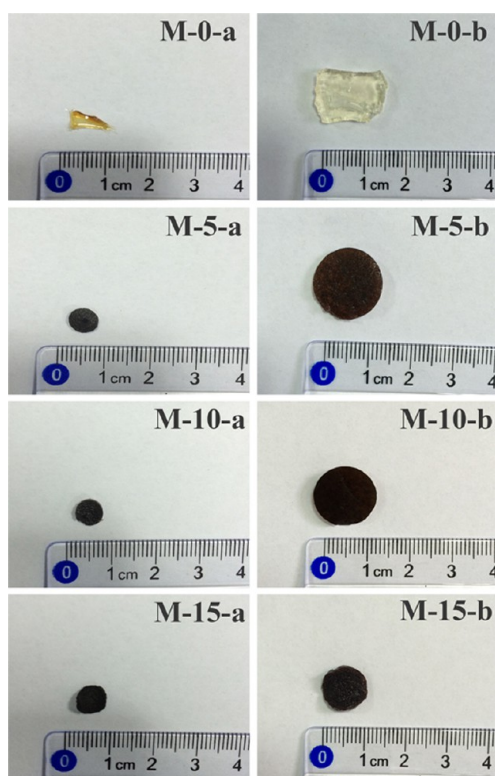**Figure 4.** Swelling curves of M-0, M-5, M-10, and M-15.

Figure 5. Photographs of hemicellulose hydrogel (M-0) and MFRHHs (M-5, M-10, and M-15) in the dry state (M-0-a, M-5-a, M-10-a, and M-15-a) and swollen state (M-0-b, M-5-b, M-10-b, and M-15-b).

one-pot preparation of MFRHHs was performed via the chemical coprecipitation of Fe_3O_4 nanoparticles during the covalent cross-linking of AcGGM. The properties of the hydrogels, such as the swelling behavior and magnetism, were defined by the Fe_3O_4 nanoparticle content.

3.1. Preparation of Magnetic-Responsive Hemicellulose Hydrogels. The as-prepared hemicellulose hydrogels and ECHHs were free-standing (Figure 1). The pure hemicellulose hydrogel was yellowish, and the magnetic field-responsive hemicellulose hydrogel was black due to the in situ formation of Fe_3O_4 particles. The pure hemicellulose hydrogel was considerably softer than the hybrid hydrogel, which is

consistent with a previous report.[37] The reason was that the addition of Fe_3O_4 particles enhanced the mechanical integrity of the polysaccharide hybrid hydrogel.

ATR-FTIR was employed to confirm the structural composition of the final magnetic field- responsive hemicellulose hydrogels. The ATR-FTIR spectra of AcGGM as well as M-0 hydrogel through M-15 hydrogel are shown in Figure 2. Pristine AcGGM exhibited characteristic C=O stretching at 1724 cm^{-1}, which corresponds to the acetylated pendant groups, some C−O−C vibrations at approximately 1022 cm^{-1} from the sugar units, a band corresponding to bound water at 1640 cm^{-1}, and a hydroxyl band at 3000−3600 cm^{-1} (Figure 2a). The disappearance of the peak at 1724 cm^{-1} indicated deacetylation of AcGGM in the M-0, M-5, M-10, and M-15 samples. The degree of deacetylation of AcGGM strongly depended on the concentration of NaOH. AcGGM can be fully deacetylated when the concentration of NaOH in the aqueous solution is higher than 1 mol/L.[33,34] NaOH is also used to form Fe_3O_4 in the current study. When more Fe_3O_4 is formed, more NaOH is consumed. Therefore, more than 1 mol/L NaOH (2.5 mol/L) was utilized in the one-pot preparation of MFRHHs. The complete deacetylation of AcGGM (Figures 2b−e) indirectly indicates that 2.5 mol/L NaOH was required for the coprecipitation of the Fe_3O_4 nanoparticles.

3.2. Thermal Properties of Magnetic-Responsive Hemicellulose Hydrogels. Because the thermal decomposition of AcGGM and Fe_3O_4 differ, the thermal behavior of MFRHHs provides insight into their composition (Figure 3). All of the hemicellulose hydrogels lost 8% (w/w) of their weight, corresponding to the evaporation of bound water below 200 °C. The hemicellulose hydrogel without Fe_3O_4 (M-0) underwent degradation between 300 and 400 °C. At temperatures above 400 °C, the thermal stability of all of the MFRHHs was lower than that of hemicellulose hydrogel (M-0). The thermal degradation between 600 and 700 °C corresponds to the loss of the Curie temperature (loss of ferromagnetism) of the magnetic Fe_3O_4 particles.[38] According to the TGA curves, the Fe_3O_4 content was 3.0, 6.6, and 9.1% (w/w) for the M-5, M-10 and M-15 hydrogels, respectively. The Fe_3O_4 content increased as the Fe_3O_4 loading increased from 5 to 15% (w/w), which indicates the successful incorporation of Fe_3O_4 into the hydrogels.

3.3. Swelling Behavior of MFRHHs. The swelling behavior of MFRHHs in water was determined by the weight gain as a function of time. The swelling ratio (SR) of the hydrogels can be controlled by altering the cross-linking densities either by the molar ratio of the cross-linker or the concentration of the functional materials.[39] Therefore, we anticipated that the SRs of the MFRHHs could be tuned by varying the amounts of the functional materials (i.e., Fe_3O_4 nanoparticles) to meet the requirements of specific applications. The Fe_3O_4 content significantly influenced the swelling behaviors of the hydrogels (Figure 4). All of the hydrogels swelled and reached equilibrium within 17 h. An increase in the amount of Fe_3O_4 nanoparticles led to a decrease in both the swelling rate and the equilibrium swelling ratio. When more Fe_3O_4 nanoparticles were formed, the water adsorption ability of the hybrid hydrogels was less than that of the pure hemicellulose hydrogels, which lowered the swelling ratios. The equilibrium SRs for the M-5, M-10, and M-15 hydrogels were 12.1, 7.4, and 2.4, respectively. As expected, these values are lower than that of the hydrogel without Fe_3O_4 nanoparticles (SR = 27.0). Swelling will open up the pores and facilitate
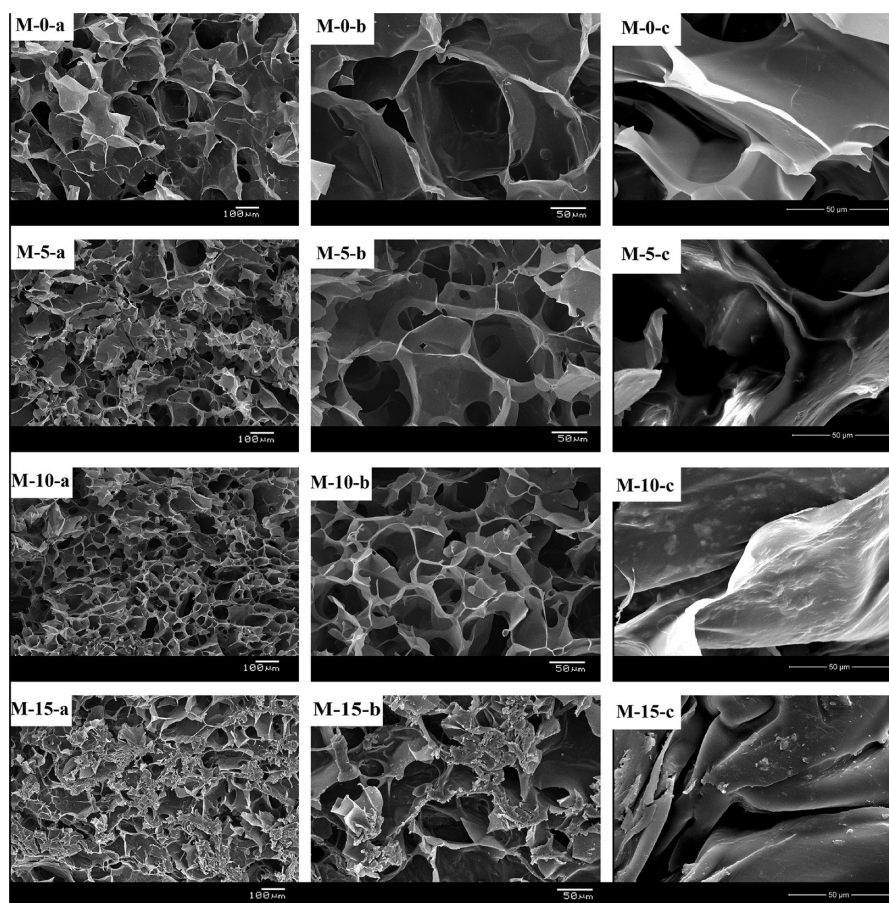
Figure 6. SEM images of cross sections of M-0, M-5, M-10, and M-15 with ×100 (M-0-a, M-5-a, M-10-a, and M-15-a), × 300 (M-0-b, M-5-b, M-10-b, and M-15-b) and ×2000 (M-0-c, M-5-c, M-10-c, and M-15-c) magnification.
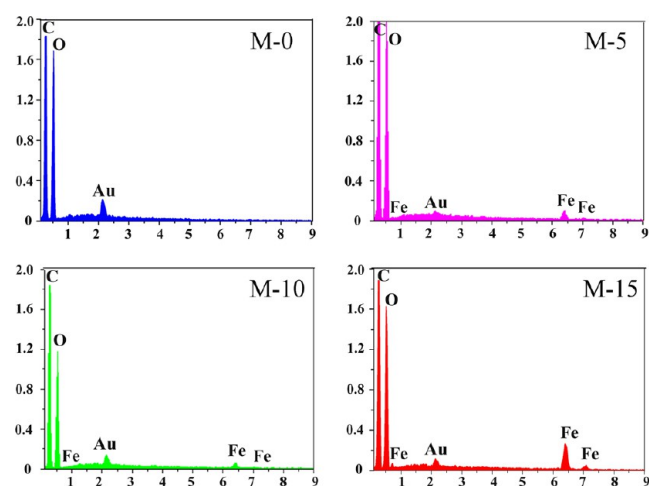

Figure 7. EDS spectra obtained from SEM for the M-0, M-5, M-10, and M-15 samples.

Figure 8. Magnetic response of magnetic particles and magnetic field-responsive hemicellulose hydrogel (M-15): without a magnetic field (left) and with a magnetic field (right).

migration by diffusion, and hence it is possible that some nanoparticles were released from the hydrogels during the swelling study, although their hydrophobicity makes this scenario less likely.

The photographs of cut pieces of the M-0, M-5, M-10, and M-15 hydrogels in both the dry and swollen states (Figure 5) indicate a volume increase following 17 h of swelling in PBS (pH = 7.2−7.4). The morphology of the hydrogels remained constant with only negligible alterations in their shape during
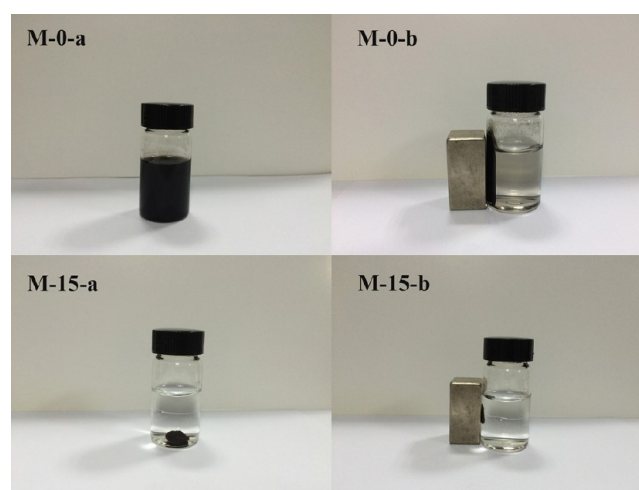
swelling, which indicated that the hydrogels exhibited good structural stability.

3.4. Scanning Electron Microscopy (SEM) of MFRHHs. The morphological changes of the hydrogels with and without Fe_3O_4 nanoparticles provide further information on their swelling behavior. The SEM images of a cross-section of the M-0, M-5, M-10, and M-15 hydrogels in the swollen state after
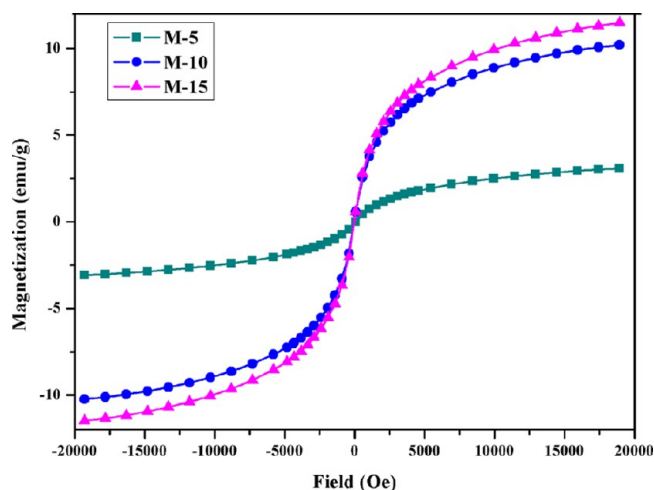
Figure 9. Magnetic hysteresis loops of the M-5, M-10 and M-15 samples at 25 °C.
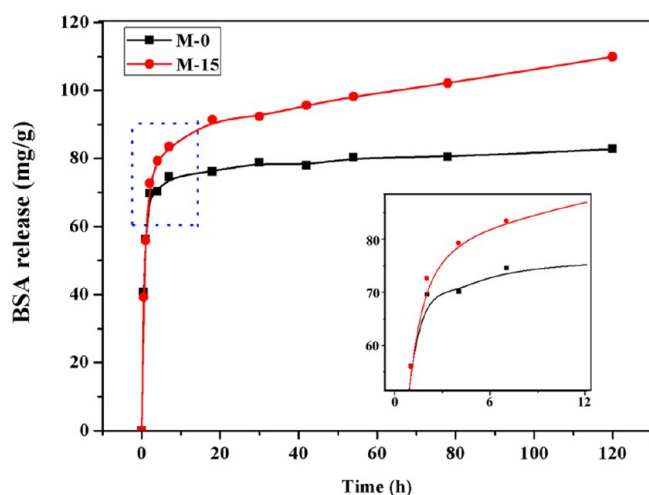

Figure 10. BSA release behavior of hemicellulose hydrogels (M-0) and MFRHHs (M-15).

freeze-drying are shown in Figure 6. All of the hydrogels possessed a homogeneous macroporous structure after 17 h of swelling, indicating that these hydrogels swelled in a homogeneous manner. The M-0 hydrogel had the largest pore size as well as the greatest ability to accommodate water. The pores and/or walls of the M-5, M-10, and M-15 samples were instead filled with and/or attached to small particles (i.e., possibly aggregates of Fe_3O_4 nanoparticles), which resulted in lower water absorption.

Figure 7 shows the energy-dispersive spectrum (EDS) from the SEM of the M-0 and M-15 hydrogels. The C, O, Au, and Fe elements were detected in the composite hydrogel. However, the hydrogels without Fe_3O_4 (M-0) only contained C, O, and Au, confirming that the MFRHHs were successfully formed by in situ synthesis of Fe_3O_4 during the covalent cross-linking of AcGGM. The presence of Au was due to the deposition of a 7 nm thick gold layer onto the hydrogels prior to observation with a SEM. According to the EDS results, the content of the Fe element in the M-15 hydrogels was 5.3% (w/w), which indicates that the Fe_3O_4 content in the M-15 hydrogels was approximately 7.3% (w/w). This result is consistent with the TGA results.

3.5. Magnetic Response of MFRHHs. The photographs of the aqueous suspension of the magnetic particles and the MFRHHs placed in a magnetic field are shown in Figure 8. The magnetic particles assembled and moved directly to the left side of the 10 mL vial where the magnetic field was applied. The MFRHHs (M-15) also possessed a magnetic response. Magnetic responsive materials have been shown useful in controlled drug release and in clinical diagnosis.[40]

The magnetization of the MFRHHs increased as the Fe_3O_4 nanoparticle content increased, indicating the successful formation of MFRHHs (Figure 9).

3.6. Protein Release Profile. The adsorption and release behavior of BSA of MFRHHs were studied. The adsorption amount of BSA by the hemicellulose hydrogels (M-0) and MFRHHs (M-15) were 100.2 and 146.5 mg/g, respectively. Therefore, the MFRHHs exhibited a much larger BSA adsorption capacity than the pure hemicellulose hydrogels. Therefore, the Fe_3O_4 nanoparticles in the adsorbent played an important role in improving the adsorption capacity due to Fe_3O_4 being available to adsorb several BSA molecules, where the NH_2 groups can bind with the orbitals of the Fe atom.[41]

Upon release of BSA, there was a burst of release during the initial stage (Figure 10) because the BSA loaded near the hydrogel surface could be immediately released from the hybrid hydrogels into the medium when the hydrogels were placed in the buffer solution (PBS, pH = 7.2−7.4). After the initial burst, the subsequent release may involve a diffusion process from the inside to the surface of the hydrogels. Based on the release curves, BSA was released more rapidly from the hydrogels during the first 12 h. More than 80 mg/g (>80%) of BSA was released from M-0, and 109 mg/g (less than 74%) of BSA was released from M-15 after 5 days. The release profiles of M-10 and M-5 were very similar to the release from sample M-15. The MFRHHs with controllable adsorption and release behaviors could be used as a carrier for drug delivery.

4. CONCLUSIONS

Stimuli-responsive hemicellulose hydrogels were created in a one-pot pathway via the in situ formation of magnetic iron oxide nanoparticles during the covalent cross-linking of hemicellulose. The ATR-FTIR and TGA results confirmed the successful incorporation of Fe_3O_4 nanoparticles into hemicellulose hydrogels. The equilibrium swelling ratios for the M-0, M-5, M-10, and M-15 hydrogels were 27.0, 12.1, 7.4, and 2.4, respectively, indicating that the content of magnetic nanoparticles controlled the swelling behaviors of the hemicellulose hydrogels. The MFRHHs also exhibited a magnetic response and superparamagnetism due to the incorporation of Fe_3O_4 nanoparticles into these hemicellulose hydrogels. The MFRHHs containing 15% (w/w) Fe_3O_4 nanoparticles exhibited a BSA adsorption capacity of 146.5 mg/g. The drug-loaded magnetic-field responsive hemicellulose hydrogels released 74% (109 mg/g) of BSA in 5 days. The MFRHHs with tunable swelling behavior as well as controllable adsorption and release properties have potential applications in the biomedical field including in controlled drug release and protein separation.

■ ASSOCIATED CONTENT

Ⓢ Supporting Information
Schemes showing the one-pot synthesis of magnetic field-responsive hemicellulose hydrogels (MFRHHs) from the hemicellulose acetylated galactoglucomannan (AcGGM).

SEM and TEM images of Fe_3O_4 magnetic particles. The Supporting Information is available free of charge on the ACS Publications website at DOI: 10.1021/acs.biomac.5b00801.

(PDF)

■ AUTHOR INFORMATION

Corresponding Author

*Tel.:+46-8-790 8274. Fax: +46-8-20 8477. E-mail: aila@kth.se.

Author Contributions

The manuscript was written through contributions of all authors. All authors have given approval to the final version of the manuscript.

Notes

The authors declare no competing financial interest.

■ REFERENCES

(1) Samchenko, Y.; Ulberg, Z.; Korotych, O. *Adv. Colloid Interface Sci.* **2011**, *168* (1−2), 247−262.

(2) Giammanco, G. E.; Sosnofsky, C. T.; Ostrowski, A. D. *ACS Appl. Mater. Interfaces* **2015**, *7* (5), 3068−76.

(3) Hoffman, A. S. *Adv. Drug Delivery Rev.* **2012**, *64*, 18−23.

(4) Edlund, U.; Ryberg, Y. Z.; Albertsson, A.-C. *Biomacromolecules* **2010**, *11* (9), 2532−2538.

(5) Maleki, L.; Edlund, U.; Albertsson, A. C. *Biomacromolecules* **2015**, *16* (2), 667−674.

(6) Xu, C.; Pranovich, A.; Hemming, J.; Holmbom, B.; Albrecht, S.; Schols, H. A.; Willfor, S. *Holzforschung* **2009**, *63* (1), 61−68.

(7) Wang, J.-P. *Proc. IEEE* **2008**, *96* (11), 1847−1863.

(8) Tzitzios, V.; Basina, G.; Bakandritsos, A.; Hadjipanayis, C. G.; Mao, H.; Niarchos, D.; Hadjipanayis, G. C.; Tucek, J.; Zboril, R. *J. Mater. Chem.* **2010**, *20* (26), 5418−5428.

(9) Yue, Q.; Zhang, Y.; Wang, C.; Wang, X.; Sun, Z.; Hou, X.-F.; Zhao, D.; Deng, Y. *J. Mater. Chem. A* **2015**, *3* (8), 4586−4594.

(10) Zhang, M.; Cao, Y.; Wang, L.; Ma, Y.; Tu, X.; Zhang, Z. *ACS Appl. Mater. Interfaces* **2015**, *7* (8), 4650−8.

(11) Nakamura, T.; Sugihara, F.; Matsushita, H.; Yoshioka, Y.; Mizukami, S.; Kikuchi, K. *Chem. Sci.* **2015**, *6* (3), 1986−1990.

(12) Smejkalova, D.; Nesporova, K.; Huerta-Angeles, G.; Syrovatka, J.; Jirak, D.; Galisova, A.; Velebny, V. *Biomacromolecules* **2014**, *15* (11), 4012−4020.

(13) Yang, X.; Du, H.; Liu, J.; Zhai, G. *Biomacromolecules* **2015**, *16* (2), 423−436.

(14) Qiang, L.; Yang, T.; Li, Z.; Wang, H.; Chen, X.; Cui, X. *Colloids Surf., A* **2014**, *456*, 62−66.

(15) Yan, S.; Zhang, X.; Sun, Y.; Wang, T.; Chen, X.; Yin, J. *Colloids Surf., B* **2014**, *113*, 302−311.

(16) Watcharin, W.; Schmithals, C.; Pleli, T.; Koeberle, V.; Korkusuz, H.; Huebner, F.; Waidmann, O.; Zeuzem, S.; Korf, H.-W.; Terfort, A.; Gelperina, S.; Vogl, T. J.; Kreuter, J.; Piiper, A. *J. Controlled Release* **2015**, *199*, 63−71.

(17) Chan, N.; Laprise-Pelletier, M.; Chevallier, P.; Bianchi, A.; Fortin, M.-A.; Oh, J. K. *Biomacromolecules* **2014**, *15* (6), 2146−2156.

(18) Tang, M.; Zhang, S.; Li, X.; Pang, X.; Qiu, H. *Mater. Chem. Phys.* **2014**, *148* (3), 639−647.

(19) Guilherme, M. R.; Oliveira, R. S.; Mauricio, M. R.; Cellet, T. S. P.; Pereira, G. M.; Kunita, M. H.; Muniz, E. C.; Rubira, A. F. *Soft Matter* **2012**, *8* (24), 6629−6637.

(20) Daniel da Silva, A. L.; Salgueiro, A. M.; Fateixa, S.; Moreira, J.; Estrada, A. C.; Gil, A. M.; Trindade, T. *MRS Online Proc. Libr.* **2012**, *1403*, 213−219.

(21) Pourjavadi, A.; Hosseini, S. H.; Seidi, F.; Soleyman, R. *Polym. Int.* **2013**, *62* (7), 1038−1044.

(22) Katagiri, K.; Ohta, K.; Sako, K.; Inumaru, K.; Hayashi, K.; Sasaki, Y.; Akiyoshi, K. *ChemPlusChem* **2014**, *79* (11), 1631−1637.

(23) Sun, X.-F.; Liu, B.; Jing, Z.; Wang, H. *Carbohydr. Polym.* **2015**, *118*, 16−23.

(24) Fathi, M.; Entezami, A. A.; Arami, S.; Rashidi, M.-R. *Int. J. Polym. Mater.* **2015**, *64* (10), 541−549.

(25) da Silva, E. P.; Sitta, D. L. A.; Fragal, V. H.; Cellet, T. S. P.; Mauricio, M. R.; Garcia, F. P.; Nakamura, C. V.; Guilherme, M. R.; Rubira, A. F.; Kunita, M. H. *Int. J. Biol. Macromol.* **2014**, *67*, 43−52.

(26) Guan, Y.; Zhang, B.; Bian, J.; Peng, F.; Sun, R.-C. *Cellulose* **2014**, *21* (3), 1709−1721.

(27) Söderqvist Lindblad, M. S.; Ranucci, E.; Albertsson, A. C. *Macromol. Rapid Commun.* **2001**, *22* (12), 962−967.

(28) Voepel, J.; Edlund, U.; Albertsson, A.-C. *J. Polym. Sci., Part A: Polym. Chem.* **2011**, *49* (11), 2366−2372.

(29) Peng, X.-W.; Ren, J.-L.; Zhong, L.-X.; Peng, F.; Sun, R.-C. *J. Agric. Food Chem.* **2011**, *59* (15), 8208−8215.

(30) Yang, J. Y.; Zhou, X. S.; Fang, J. *Carbohydr. Polym.* **2011**, *86* (3), 1113−1117.

(31) Sun, X.-F.; Wang, H.-h.; Jing, Z.-x.; Mohanathas, R. *Carbohydr. Polym.* **2013**, *92* (2), 1357−1366.

(32) Zhao, W.; Glavas, L.; Odelius, K.; Edlund, U.; Albertsson, A.-C. *Polymer* **2014**, *55* (13), 2967−2976.

(33) Zhao, W.; Glavas, L.; Odelius, K.; Edlund, U.; Albertsson, A.-C. *Chem. Mater.* **2014**, *26* (14), 4265−4273.

(34) Zhao, W.; Nugroho, R. W. N.; Odelius, K.; Edlund, U.; Zhao, C.; Albertsson, A.-C. *ACS Appl. Mater. Interfaces* **2015**, *7* (7), 4202−4215.

(35) Jacobs, A.; Dahlman, O. *Biomacromolecules* **2001**, *2* (3), 894−905.

(36) Sparks, J.; Scholz, C. *Biomacromolecules* **2009**, *10* (7), 1715−1719.

(37) Yadav, M.; Rhee, K. Y.; Park, S. J.; Hui, D. *Composites, Part B* **2014**, *66*, 89−96.

(38) Cao, X.; Prozorov, R.; Koltypin, Y.; Kataby, G.; Felner, I.; Gedanken, A. *J. Mater. Res.* **1997**, *12* (2), 402−406.

(39) Maleki, L.; Edlund, U.; Albertsson, A.-C. *Carbohydr. Polym.* **2014**, *108*, 281−290.

(40) Luo, X.; Liu, S.; Zhou, J.; Zhang, L. *J. Mater. Chem.* **2009**, *19* (21), 3538−3545.

(41) Wang, Y.; Wang, X.; Luo, G.; Dai, Y. *Bioresour. Technol.* **2008**, *99* (9), 3881−3884.